PELO Facilitates PLK1- Induced the Ubiquitination and Degradation of Smad4 and Promotes the Progression of Prostate Cancer

Ping Gao (ping.gao2016@outlook.com)
Shaanxi Normal University https://orcid.org/0000-0003-1383-3290
Jinglan Hao
Shaanxi Normal University
Qianwen Xie
Shaanxi Normal University
Guiqin Han
Shaanxi Normal University
Binbing Xu
Shaanxi Normal University
Hang Hu
Shaanxi Normal University
Naer Sa
Shaanxi Normal University
Xiaoming Dong
Shaanxi Normal University

Article

Keywords: PLK1, PELO, Smad4, Prostate Cancer, PLK1 Inhibitor

Posted Date: November 8th, 2021

DOI: https://doi.org/10.21203/rs.3.rs-883075/v1

Version of Record: A version of this preprint was published at Oncogene on April 18th, 2022. See the published version at https://doi.org/10.1038/s41388-022-02316-8.

Abstract

PLK1 and Smad4 are two important factors in prostate cancer initiation and progression. They have been reported to play the opposite role in Pten-deleted mouse, one is an oncogene, the other is a tumor suppressor. Moreover, they could reversely regulate the PI3K/AKT/mTOR pathway and the activation of MYC. However, the connections between PLK1 and Smad4 have never been studied. Here, we showed that PLK1 could interact with Smad4 and promote the ubiquitination and degradation of Smad4 in PCa cells. PLK1 and PELO could bind to different domain of Smad4 and formed a protein complex. PELO facilitated the degradation of Smad4 through cooperating with PLK1, thereby resulting in proliferation and metastasis of prostate cancer cell. Changes in protein levels of Smad4 led to the alteration of biological function that caused by PLK1 in prostate cancer cells. Further studies showed that PELO upregulation was positively associated with high grade PCa and knockdown of PELO expression significantly decreased PCa cell proliferation and metastasis in vitro and vivo. PELO knockdown in PCa cells could enhance the tumor suppressive role of PLK1 inhibitor. In addition, blocking the interaction between PELO and Smad4 by using specific peptide could effectively inhibit PCa cell metastasis ability in vitro and vivo. Overall, these findings identified a novel regulatory relationship among PLK1, Smad4 and PELO, and provided a potential therapeutic strategy for advanced PCa therapy by co-targeting PLK1 and PELO.

Background

Prostate cancer (PCa) is one of the leading cancer types in men in the world. Even though the survival rate of localized PCa is high, but the lethal rate will become higher when it relapses and transformed into metastatic tumor cells [1, 2]. Polo-like kinase 1 (PLK1) plays an important role in regulating cell cycles, such as centrosome maturation, spindle assembly, mitotic exit and cytokinesis. The increased PLK1 expression in Pten-deleted mouse could induce prostate cancer formation [3]. Targeting Plk1 inhibits the activity of the PI3K/AKT/mTOR signaling pathway [4]. Higher PLK1 expression has been identified positively associated with high grade PCa [5] and considered as a therapeutic target in multiple cancer types [6]. Thus far, PLK1 inhibitors has already been applied to treat multiple cancers in clinical trials [7]. Unlike PLK1, Smad4 was identified as a tumor suppressor in human PCa, Smad4 deletion drives progression of Pten-deficient mouse prostate tumor to highly aggressive prostate cancer [8]. Interestingly, PLK1 induces MYC phosphorylation and protein accumulation [9], whereas Smad4 is a transcription suppressor of MYC in cancer cells [10]. Whether there are any relationships between the oncogenic factor PLK1 and the tumor suppressor Smad4 in prostate cancer still unclear.

PELO, is an indispensable gene in the cell meiotic division process and mice embryonic development [11]. PELO knockout in mice results in early embryonic lethality because it plays a crucial role in cell mitosis. The significant role of PELO in ribosome-associated mRNA quality control mechanisms has been first found in yeast [12]. Although it was reported to be a tumor suppressor in breast cancer [13], the function of PELO in prostate cancer initiation, progression and metastasis have not yet been studied.

In the present study, we investigated PLK1 evoked oncogenic transformation related events. We identified the crucial role of PLK1 in regulating the ubiquitination and degradation of Smad4. Our findings supported that PELO was an important factor to facilitate PLK1-induced the ubiquitination and degradation of Smad4, thereby resulting in proliferation and metastasis of prostate cancer cell. We further proved that PELO was highly expressed in PCa tissues, knockdown of PELO markedly inhibited cell growth and metastasis ability. These findings expanded our understanding of regulatory relationship among PLK1, Smad4 and PELO in prostate cancer, and provided new insights into potential PCa treatments targeting PLK1 and PELO.

Results

PLK1 promoted the ubiquitination and degradation of Smad4 in prostate cancer.

To explore the relationship between PLK1 and Smad4, we first investigated whether there was direct interaction between PLK1 and Smad4 through Co-immunoprecipitation experiment. The result indicated that PLK1 strongly interacts with Smad4 (Figure. 1A). Next, we found that the expression level of Smad4 was gradually decreased when the amount of PLK1 increased in PCa cells (Figure. 1B). Accordingly, PLK1 inhibitor RO3280 (RO) [14] could elevate the protein level of Smad4 in PC3 cells in a dose-dependent manner (Figure. 1C). To investigate the molecular mechanism by which PLK1 regulated Smad4 protein expression level, we assessed the half-life of Smad4 protein. PLK1 overexpression PC3 cells or control cells were treated with the protein synthesis inhibitor cycloheximide (CHX) at different time points. The results showed that PLK1 overexpression promoted the protein degradation of Smad4 and shortened the half-life of Smad4 protein (Figure. 1D). However, PLK1 inhibitor RO3280 in PC3 cells led to a reduced degradation of Smad4 protein. (Figure. 1E). We then found that the degradation of Smad4 protein caused by PLK1 was obviously inhibited by the ubiquitination-proteasome pathway inhibitor MG132, suggesting that PLK1 attenuated Smad4 protein stability through the ubiquitination-proteasome pathway (Figure. 1F).

To further validate the results, we co-expressed HA-ubiquitin, MYC-Smad4 or Flag-PLK1 in HEK293T cells. Smad4 protein was immunoprecipitated by MYC antibody, and the ubiquitinated protein was detected with HA antibody. The results indicated that PLK1 overexpression could strongly strengthen the ubiquitination of Smad4 protein in a dose-dependent manner. (Figure. 1G). Then we treated PC3 cells with increasing amount of RO and measured the endogenous ubiquitin Smad4 protein that was immunoprecipitated by the Smad4 specific antibody. We found that RO led to the decreased ubiquitination of Smad4 protein in a dose-dependent manner (Figure. 1F). The results further validated that PLK1 accelerated the ubiquitination and degradation of Smad4 though the ubiquitination-proteasome pathway.

Smad4 reversed the biological function of PLK1 in prostate cancer.

To determine whether the amount of Smad4 protein is important for PLK1 to perform its oncogenic role in PCa, we performed rescue experiment. PC3 cells were treated with RO for 12 h, followed by transfection

with Smad4 siRNA. Then cell proliferation was measured by XTT colorimetric assays. We found that RO significantly decreased the cell proliferation and metastasis both in PC3 and LNCaP cells, but knockdown of Smad4 rescued cell proliferation and metastasis (Figure. 2A,B,E,F and Supplementary Fig. S1A,B,E). Consistent with these results, PLK1 overexpression evidently enhanced the cell proliferation and metastasis both in PC3 and LNCaP cells, but Smad4 elevation rescued cell proliferation and metastasis. (Figure. 2C,D,G,H and Supplementary Fig. S1C,D,F). We further measured the expression levels of epithelial-mesenchymal transition markers, cell growth and metastasis related genes in PC3 cells. We found that Ectopic expression of Smad4 could reverse the mRNA levels of *E-Cadherin*, *N-Cadherin*, *Vimentin*, *MMP9* and *CCND1* in PLK1 overexpressed PC3 cells (Figure. 2I). These findings proved that PLK1 play the critical role in cell proliferation and metastasis by regulating Smad4 expression levels in PCa.

PLK1 formed a protein complex with Smad4 and PELO in PCa.

To explore the Smad4-interacting proteins in prostate cancer cells, we initially performed an IP-MS assay by using specific anti-smad4 antibody to identify Smad4-binding proteins in PC3 cells (Figure. 3A). Then, we performed Kyoto Encyclopedia of Genes and Genomes (KEGG) pathway enrichment analysis to find the main functional pathways of the Smad4-interacting proteins. Among these Smad4-interacting proteins, 70 proteins are enriched in Spliceosome pathway, 24 proteins enriched in mRNA surveillance pathway and 22 proteins enriched in Ribosome pathway (Figure. 3B). Protein–protein interaction (PPI) networks result showed these proteins connect the pathways of mRNA surveillance, RNA transport, RNA degradation and Biosynthesis of amino acids together (Supplementary Fig. S2A). One of these proteins, PELO, which belongs to mRNA surveillance pathway but has less connections with other proteins in this pathway (Supplementary Fig. S2B). Then we ectopically expressed MYC-Smad4 and Flag-PELO in 239T cells and performed immunoprecipitation experiment using antibodies specifically identify MYC or Flag. The results proved that Smad4 could interact with PELO (Figure. 3C, D). Glutathione *S*-transferase (GST) pull down assay further confirmed that there is direct interaction between Smad4 and PELO (Supplementary Fig. S2C). Considering both of PLK1 and PELO could interact with Smad4, we then explored the associations between PLK1 and PELO and verified that PELO could interact with PLK1 (Figure. 3E).

To determine which region of Smad4 is required for PLK1 or PELO binding, Myc-tagged full-length Smad4 and deletion mutants (Figure. 3F) were co-transfected into 293T cells with PLK1 or PELO expression vector. Immunoprecipitations were performed using anti-Myc antibody. The results showed that functional domain Linker 2 of Smad4 was essential for the binding of PLK1, whereas PELO could bind to the MH2 domain of Smad4 (Figure. 3G, H). In this way, our results indicated the associations between PLK1, PELO, and Smad4 occur at non-overlapping regions of the proteins. These data prompted us to hypothesize that Smad4 might form complex with PLK1 and PELO. Smad4-specific antibody was used to immunoprecipitate PC3 cells extracts and the immunoprecipitated proteins were analyzed by Western blotting. As expected, PLK1 and PELO could indeed be coimmunoprecipitated (Figure. 3I). Together, these results indicated that PLK1 and PELO could bind to Smad4 simultaneously through different regions,

forming a protein complex. However, the role of PLK1/PELO/Smad4 complex in PCa need to be further explored.

PELO facilitated PLK1-induced the ubiquitination and degradation of Smad4

To investigate the role of PELO in this proteins complex, we next designed short hairpin RNAs that could specifically knock down PELO expression other than ITGA1 in PCa cell lines (Supplementary Fig. S4A, B). Interestingly, similar with PLK1, knockdown of PELO also markedly elevated the protein level of Smad4 (Figure. 4A). Then we evaluated whether PELO influences PLK1-induced degradation of Smad4. As shown in Figure 4B, PELO knockdown blocked PLK1-induced protein degradation of Smad4 in PC3 cells to a significant extent.

To explore whether PELO regulates the interaction between PLK1 and Smad4, PC3 cells transfected with PELO overexpression lentivirus or PELO shRNA lentivirus, and immunoprecipitations were performed with Smad4 antibody. The results showed that overexpression of PELO enhanced the interaction between PLK1 and Smad4 (Figure. 4C), whereas knockdown of PELO attenuated the interaction between PLK1 and Smad4 (Figure. 4D). Next, we evaluated whether PELO influences PLK1-induced ubiquitination of Smad4. We found that overexpression of PELO could enhance PLK1-induced the ubiquitination and degradation of Smad4 in a dose-dependent manner (Figure. 4E). Consist with this result, knockdown of PELO partially blocked PLK1-induced ubiquitination of Smad4 in PC3 cells (Figure. 4F). These results indicated that PELO was essential for mediating the interaction between PLK1 and Smad4, and PLK1-induced the ubiquitination and degradation of Smad4.

Increased expression of PELO positively associated with high risk of PCa.

To determine the role of PELO in PCa initiation and progression, we first examined the protein level of PELO in clinical prostate cancer samples. Hence, we analyzed the mRNA level of PELO in published prostate cancer sample cohorts. PELO was highly expressed in high Gleason score in samples from GSE134051 (Figure. 5A). Importantly, PELO was found highly expressed in high stage and metastatic PCa samples compared with in primary samples in several cohorts (Figure. 5B, C and Supplementary Fig. S3D,F,G). Interestingly, we found that PELO was highly expressed in liver metastasis samples compared with lymph node metastasis samples in cohort GSE74685 (Supplementary Fig. S3E). We also found that PELO expression was correlated with the overall survival (Figure 5D) and disease-free survival (Figure 5E) of PCa patients in the TCGA cohorts. Then, we collected two cohorts of prostate samples, one cohort includes 3 normal prostate tissues, 50 adjunct normal samples and 94 tumor samples, the other involves 42 adjunct normal samples and 95 primary tumor samples. By performing immunohistochemistry (IHC) analysis on the PCa tissue chips, we observed that PELO was significantly upregulated in tumor samples in comparison with the normal and adjunct normal prostate tissue samples in both of the two cohorts (Figure 5F, G and Supplementary Fig. S3A-C). Moreover, the protein level of PELO was highly expressed in high Gleason score 7–9, a vital parameter to evaluate PCa progression, compared with low Gleason score 6 PCa tissues (Figure 5H). These results indicated that PELO expression strongly elevated during PCa progression and was associated with shorter survival of patients.

We next explore the biological function of PELO in PCa cells. The cell proliferation rate was significantly decreased when diminishing PELO protein level in PCa cell lines such as LNCaP, PC3 cells and Du145 cells (Figure. 5I, J and Supplementary Fig. S4D-E) even though knockdown of PELO in RWPE1 cells has no effect on cell growth (Supplementary Fig. S4C). PC3 and Du145 cells belong to advanced PCa cell lines, knockdown of PELO expression in those two cell lines could strongly restrain cell migration and invasion ability (Figure. 5K,L and Supplementary Fig. S4F-K). Inhibition of PELO expression in PC3 cells could also apparently decrease cell colony formation ability (Supplementary Fig. S4L-M). To investigate in vivo metastatic capacity of PELO, we further validate the impact of PELO on organ colonization ability of human prostate tumor cells in NSG mouse model. We injected the control PC3 cells and PELO deletion PC3 cells into 5 NSG mice through the tail veins, respectively. All mice were killed 40 days after cells injection, except for three mice in the control group that to be killed earlier due to their poor condition. Histopathological analysis showed that the average size and amount of tumor lesions in the lungs and livers in mice injected with PC3-shPELO subline cells were significantly smaller and lower than in the control mice (Figure. 5M,N). Taken together, these data demonstrated that PELO deletion could strongly suppress cell growth and metastasis in PCa cells, and PELO might be a novel therapeutic target for the treatment of advanced PCa in clinical.

Knockdown of PELO enhanced the tumor suppressive function of PLK1 inhibitor RO

To determine whether PELO could cooperate with PLK1 to regulate prostate cancer cell growth, PC3 cells were transfected with PELO shRNA lentivirus or control lentivirus, followed by treatment with RO and tested protein level of Smad4, cell proliferation and metastasis. The results showed that inhibiting the expression of PLK1 and PELO at the same time obviously led to the higher protein level of Smad4 compare with inhibition of the expression of PLK1 or PELO (Figure. 6A). As expected, either RO or knockdown of PELO in PC3 and Du145 cells reduced cell growth and metastasis, but knockdown of PELO in PC3 cells treated with RO significantly restrained cell growth (Figure. 6B,C) and metastasis (Figure. 6D-G) to a significant extent. These results suggested that PELO cooperate with PLK1 to enhance prostate cancer cell growth and metastasis.

Blocking interaction between PELO and Smad4 by specific peptide inhibited PCa cell metastasis.

To determine which domain of PELO is required for binding Smad4, full-length PELO and deletion mutants of PELO were cloned into vector pCMV-FLAG, expressing Flag-tagged proteins. 293T cells were co-transfected with Myc tagged-Smad4 and PELO deletion mutants or control vector. Immunoprecipitations were performed with anti-Flag antibody. As shown in (Figure. 7A), the 137-268 amino acids of PELO were required for Smad4 binding. To determine whether blocking the interaction between PELO and Smad4 influenced cell metastasis in vivo, we designed several peptides targeting the 137-268 amino acids of PELO and picked one peptide which could effectively block the interaction between PELO and Smad4 in PC3 cells (Figure. 7B). Interestingly, Blocking the interaction between PELO and Smad4 apparently increased the protein level of Smad4 (Figure. 7C). To investigate whether the peptide suppresses tumor metastases in vivo, PC3 cells were injected into 15 NSG mice. 7 mice were

injected with PBS and the others were injected with peptide through tail vein injection every two days. Mice will be killed when they were under poor conditions and calculated as death. There were no mice left in control group and 5 mice left in the peptide injection group at day 50 after the cell injection. We found that the surface of the lungs is smoother and the white spots at the surface of the liver are less in the mice injected with peptide compared with mice injected with PBS (Figure. 7D). We also observed that mice (n = 8) that injected with peptide via tail vein at a dose of 10 mg/kg remarkably increased survival rate compared with mice injected with PBS (n = 7) (Figure.7E). Moreover, Histopathological analysis showed a remarkably decreased burden of tumors in lungs and livers in the mice treated with peptide compared with mice injected with PBS (Figure. 7F-I). Taken together, these results indicated that the peptide injection could significantly prevent the tumor cells metastasize to the lung and liver in mice.

Discussion

In Pten-deleted mouse, high expression level of PLK1 induces cancer formation, whereas high expression level of Smad4 performs the role of tumor suppressor. However, the connections of those two important factors in prostate cancer initiation and progression have never been reported. In this study, we first deeply investigated the relationship between PLK1 and Smad4 thoroughly. Our results proved that PLK1 and PELO could directly bind to different domains of Smad4 and formed a protein complex. PLK1 promotes the ubiquitination and degradation of Smad4 in PCa cells with the help of PELO. The biological impact of PLK1 inhibitor on cell growth and metastasis could be restored by knockdown of Smad4.

PLK1 and Smad4 are important factors for the initiation and progression in multiple cancer types [15, 16, 17]. PLK1 was found to act upstream of PI3K/AKT/mTOR signaling pathway [4], whereas another study proved that Smad4 could deactivate the PI3K/mTOR pathway by interacting with the P85 subunit of PI3K in ovarian cancer [18]. PLK1 and Smad4 oppositely regulate MYC activity [9, 10]. Moreover, the Smad4 mutated HNSCC cell lines have showed the resistance characters for PLK1 inhibitor [19]. All these previous studies suggested that there is an antagonistic function between Smad4 and PLK1 and build strong research basis for our present study. Here, our findings further unveiled the reason of why Smad4 mutated cells have showed resistant to PLK1 inhibitor. We provided strong evidence to support that PLK1 could indeed induce the ubiquitination and degradation Smad4 with the help of PELO. The degradation of Smad4 should be crucial for PLK1 to switch on its downstream events. Our present study supplies more clues for applying the PLK1 inhibitors in clinical trials.

In this study, we also explored the role of PELO in PCa initiation and progression for the first time. Contrast to the biological role in breast cancer, PELO is positively associated with advanced PCa. We further proved that PELO was highly expressed in prostate cancer tissues, especially in metastatic tumors. Importantly, knockdown of PELO markedly decreases the metastasis ability of advanced PCa cells in vitro and vivo. Blocking the interaction of PELO and Smad4 could prevent the degradation of Smad4 and inhibit cell metastasis in vitro and in vivo. Interestingly, unlike in tumor cells, depletion of PELO expression in normal prostate epithelial cells had no impact on cell proliferation. Recent studies indicated that inactivation of PELO in mammalian tissues disrupt the translational control and activate

mTOR signaling to compensate for impaired or reduced availability of ribosomes [20]. These findings suggested that the signaling pathways of PELO in normal and tumor cells are quite different. Exploring the role of PELO during tumor initiation will provide us more clues to understand the transformation of cells from normal to tumor status.

In the last decades, inhibitors and peptide therapeutics developed fast in clinical trials and pharmaceutical market [21, 22, 23]. Several PLK1 inhibitors has been developed and applied in clinical trials [24, 25]. However, preclinical success with PLK1 inhibitors has not translated well into clinical success, this might be due to the specificity of the inhibitors still need to be improved [26, 27]. Overall, our studies pinpointed a novel mechanism of Smad4 degradation in prostate cancer and proved that a combination of PLK1 inhibitor with inhibition of PELO could synergistically enhance the effect of inhibiting tumor cell growth and metastasis. All these finding provided a potential therapeutic strategy for advanced PCa treatment by co-targeting PLK1 and PELO in future studies.

Material And Methods

Cell culture

All cell lines were originally purchased from the American Type Culture Collection (ATCC) and none of these cell lines were found to be contaminated with mycoplasma during our study. 293T cells were grown in DMEM (Invitrogen, catalog no. 10569010); RWPE-1 cells were cultured with keratinocyte serum-free medium (Invitrogen, catalog no. 10724011) with bovine pituitary extract and human recombinant EGF; LNCaP and DU145 cells were grown in RPMI1640 (Merck, catalog no. R8758); PC3 cells were cultured in F-12 Kaighn's Modification (HyClone, catalog no. SH30526.01). All media were supplemented with 10% fetal bovine serum (Gibco, catalog no. 10099-141C) and with antibiotics (Thermo Fisher Scientific, catalog no. 15140122).

Immunoprecipitation

Immunoprecipitation was performed as described previously [28]. Briefly, for transfection-based co-immunoprecipitation assays, 293T cells were transfected with the indicated plasmids using Lipofectamine 2000 (Invitrogen, catalog no. 11668019) lysed and immunoprecipitated with anti-FLAG antibody (Sigma-Aldrich, catalog no. F3165) or anti-MYC antibody (Thermo Fisher Scientific, catalog no. MA1-980) combined agarose beads, Cells lysed and immunoprecipitated with anti-Smad4 antibody (Abclonal, catalog no. A19116) combined agarose beads for 12 h at 4°C. The beads were washed three times with the lysis buffer and eluted in SDS sample loading buffer. The eluted proteins were separated by SDS-PAGE, transferred to PVDF membranes (Millipore, catalog no. ISEQ00010) and detected in western blots with appropriate primary antibodies coupled with HRP-conjugated secondary antibody by chemiluminescence (Pierce, catalog no. 32106). For detection of the interaction of endogenous proteins, whole cell extracts were immunoprecipitated with specific antibodies overnight at 4°C. Normal IgG was used as a negative control. After extensive washes, the immunoprecipitates were resolved with SDS sample loading buffer for Western blot analysis.

Ubiquitination of Smad4.

HEK293T cells were transfected with the indicated constructs. 36 h after transfection, cells were harvested and lysed in lysis buffer. Anti-HA (ABclonal: AE008) antibody was used to detect polyubiquitinated Smad4. For detecting the endogenous ubiquitination of Smad4, PLK1 overexpression in PC3 cells were lysed in lysis buffer. Then, the ubiquitination of Smad4 was analyzed by immunoprecipitated with anti-Smad4 (ABclonal: A19116) antibody and immunoblotted with anti-Ub (ABclonal: A19686) antibody or anti-Smad4 antibody.

Cycloheximide (CHX) chase assay.

Cells were incubated in 50 μg/ml cycloheximide (Cell Signaling Technology, catalog no. 2112) for indicated times. Then, cells were harvested and lysed in 2 × Loading sample buffer**.** Protein level was determined by western blot analysis.

Western blot

Cells pellets were harvested and resuspended in lysis buffer (600mM NaCl, 1% Triton X-100 in PBS, 1 x protease inhibitor). Protein concentration was measured using the BCA protein assay kit (Thermo Fisher Scientific, catalog no. 23227). Western blot analysis was performed in accordance with standard procedures. Anti-PELO antibody (ab140615) was purchased from Abcam; anti-PELO (SAB1401719) and anti-FLAG (F3165) antibodies were purchased from Merck; anti-Smad4 (A19116), anti-HA (AE008), anti-Ubiquitin (A19686), anti-GAPDH (AC002) and anti-MYC tag (AE010) antibodies were purchased from ABclonal; anti-PLK1 antibody (4513S) was purchased from Cell Signaling Technology; anti-MYC (MA1-980), anti-V5 (MA5-15253), anti-ITGA1 (PA5-79525) and HRP-conjugated secondary antibodies were purchased from Thermo Fisher. Signals were visualized with the Super Signal West Pico PLUS Chemiluminescent Substrate kit (Pierce, catalog no. 34577).

Immunohistochemistry (IHC) assays

To explore the expression of PELO in PCa tissues and adjacent tissues, two PCa tissue chips (Catalog No. HProA 150CS01, HProA150PG02) were purchased from Outdo Biotech (Shanghai, China). We first deparaffinized and rehydrated the tissue chips, retrieval antigen 5 min at 121°C, blocked endogenous enzyme activity 30 min at room temperature using 3% H_2O_2-methanol, blocked the chips 1 h with 5% BSA. We incubated the chips with the PELO primary antibody (Abcam, catalog no. ab140615) (diluted at 1:50) overnight at 4 °C. Then we incubated the tissue chips with EnVision-HRP secondary antibody for 1 h, the signals were detected by diaminobenzidine followed by hematoxylin counterstaining. Aperio ScanScope slide scanner was used for viewing the signals. Of note, the result was assessed according to the intensity of staining (0, 1+, 2+, and 3+) and the percentage of positive cells (0 (0%), 1 (1–25%), 2 (26–50%), 3 (51–75%), and 4 (76–100%)) by two experienced pathologists. Finally, the final staining score was calculated and analyzed.

Xenograft tumor model and in vivo metastasis analysis

30 male athymic nude mice at 4 weeks of age were used according to the protocols approved by the ethical committee of Shaanxi Normal University. Briefly, for in vivo metastasis analysis, male nude mice (5 per group) were injected i.v. via the tail vein with 1×10^6 PC3 sublines (control shRNA, shPELO-1 and shPELO-2). Six weeks later, nude mice were sacrificed, and the lung and liver metastases were examined by H&E staining. For the peptide experiment, 15 male nude mice were injected with 1×10^6 PC3 cells through tail vein, after 2 days, 7 nude mice were injected with PBS through tail vein every 2 days, the others were treated with peptide every 2 days. 50 days later, the liver and lung were dissected from each of the mice, then H&E staining was used to exam the metastases status.

RNA isolation and real-time PCR

Total RNA was extracted using RNeasy Mini kit (Tiangen, catalog no. DP430) according to the manufacturer's instructions. First strand cDNA was synthesized using 1 ug of total RNA and Superscript II (Thermo Fisher Scientific, catalog no. 4368814). Real-time quantitative PCR was performed in triplicates with SYBR Green qPCR mix (Thermo Fisher Scientific, catalog no. 4472908). The relative amount of specific mRNA was normalized to GAPDH.

Cell viability and proliferation assays.

Cells treated with PELO shRNA or control shRNA lentivirus (1×10^3 per well) were seeded in 96-well plates. Cell viability and proliferation were determined with XTT assays (Roche, catalog no. 11465015001) at designed time points by measuring the absorbance at 450 nm, following the manufacturer's instructions. Values were obtained from three replicate wells for each treatment and time point. The results are representative of three independent experiments. Significance was calculated by a two-tailed *t* test.

Transwell invasion and migration assay

Standard 24-well Boyden invasion chambers (BD Biosciences) were used to assess cell invasiveness following the manufacturer's suggestions. Briefly, cells were trypsinized, rinsed twice with PBS, resuspended in serum-free medium at 2.5×10^5 cells/ml. 200 µl of cell suspension was transferred into 8-µm Transwell inserts (Corning Costar, catalog no. 3422) with (invasion) or without (migration) 100 µl Matrigel (diluted with serum free medium to 250µg/ml) coating (BD Biosciences, catalog no.356230). 10% serum-containing medium was added in the lower chambers. Following 48 h incubation, chambers were fixed in 3.7 % formaldehyde, after permeabilized with methanol, stained with Wright-Giemsa (Sigma-Aldrich, catalog no. WG16) for manual counting. A two-tailed *t*-test was employed to perform statistical analysis from three replicate inserts.

Chromatin immunoprecipitation (ChIP).

The ChIP experiment was performed as previously described [29]. Briefly, PC3 cells were crosslinked with 1 % formaldehyde (Merck, catalog no. F8775) and stopped the reaction with 125 mM glycine (Merck,

catalog no. G8898). The nuclei were isolated from cells and then suspended in SDS lysis buffer. Nuclear extracts were sonicated to generate an average size of 400bp chromatin fragment. In each reaction, 6 μg of anti-Smad4 antibody (ABclonal, catalog no. A19116), anti-TEAD1 antibody (ABclonal, catalog no. A6768) or normal rabbit IgG (CST, catalog no. #2729) were incubated with 70 μl of Dynabead protein G (Invitrogen, catalog no. 10004D) slurry in IP buffer for 12 h. Then the fragmented chromatin was incubated with bead/antibody complexes overnight. After washing and reverse-crosslinking, the precipitated DNA was purified with MinElute PCR Purification Kit (Qiagen, catalog no. 28006) and the target DNA fragments were analyzed by qPCR. Enrichment was calculated relative to input.

Lentiviral constructs, lentivirus production and infection.

The shRNA constructs targeting *PELO* were ordered from Merck. In detail, 293T cells were trypsinized and seeded into 3.5-cm plates with normal DMEM medium containing 10 % FBS, 1 % penicillin and streptomycin. The normal DMEM medium was replaced with 2 ml low glucose DMEM (Invitrogen, catalog no. 21885025) before transfection. For second generation lentiviral production, 1.5 μg shRNA construct, 0.375 μg pMD2.G (envelope plasmid), and 1.125 μg psPAX2 (packaging plasmid) were diluted to 100 ul using Opti-MEM (Invitrogen, catalog no. 11058-021) and combined with 100 ul Opti-MEM containing 8 μl Lipofectamine 2000 (Invitrogen, catalog no. 11668019). This mixture was incubated at room temperature for 20 min and added to the 2 ml medium covering the 293T cells. The medium was changed to fresh medium after 24 h and the virus-containing medium was harvested every 24 h up to three times. Lentivirus was passed through 0.45 μm filter unit and stored at −80 °C. For viral transduction, Viral supernatants containing 8 μg/ml polybrene (Merck, catalog no. H9268) were added to PCa cells that were seeded 24 h before infection at 70–80% confluence. For lentivirus-mediated knockdown experiment, virus was removed and replaced by normal medium with antibiotics after 24 h, after which cells were selected with 1 μg/ml puromycin (Merck, catalog no. P9620). When uninfected control cells were completely killed, the target cells were cultured in normal growth medium with 0.5 μg/ml puromycin for further experiments.

GST Pull-down Assay

PELO full length was cloned in frame with the glutathione S-transferase (GST) gene of pGEX-6P-1 and the resulting GST fusion proteins were expressed in *Escherichia coli* BL21, induced by 0.1 mM isopropyl-b-D-thiogalactopyranoside (IPTG) and solubilized from bacteria in lysis buffer (1% Triton X-100 in PBS) by sonication. After centrifugation for 10 minutes at 4°C, the supernatant was incubated with the glutathione-Sepharose 4B beads (Thermo Fisher Scientific, catalog no. 16100) at 4°C overnight. Beads were harvested through centrifugation and washed three times in cold PBS to remove nonspecific binding. GST and GST-fusion proteins were bound to glutathione-Sepharose beads followed by SDS-PAGE. The PC3 cell lysates were treated with DNase I (Thermo Fisher Scientific, catalog no. 18047019) for 30 minutes at 37°C to remove the genomic DNA contamination before mixed with GST fusion protein which adsorbed to Sepharose beads. The binding reaction was carried out overnight at 4°C in 1 mL binding buffer (20 mmol/L Tris-HCl at pH 8.0, 150 mmol/L NaCl, 1 mmol/L EDTA, 10% glycerol and 0.1%

NP-40). After extensive washing, specifically bound proteins were subjected to 10% SDS-PAGE followed by western blot analysis.

Soft agar assays

About 400 PC3-control, PC3-shPELO-1 and PC3-shPELO-2 cells were suspended in 0.2 ml of prewarmed 0.35% SeaPlaque agarose/MEM/5% fetal bovine serum and pipetted on top of 0.3 ml of 0.7% SeaPlaque agarose/MEM/5% fetal bovine serum gelled onto a well of a 24-well plate, then 0.4ml medium was added on top of the cells. Cells were incubated for 15 days, at 37 °C and 5% CO_2, and fresh medium was changed every three days. The colony spots were counted through eye vision.

Statistical analysis

All statistical analyses were performed using GraphPad Prism version 5.0 software (GraphPad, San Diego, CA, USA). Data were obtained from the cBioPortal for Cancer Genomics [30, 31], and GEO database [32, 33]. Statistical tests for patients with gene expression were calculated using Mann-Whitney U test. Kaplan Meier survival analysis was used to assess the impact of gene expression levels on prostate cancer prognosis and survival. *P* value < 0.05 was considered to be statistically significant, all error bars in graphical data represent mean ± SD.

Declarations

Acknowledgements

We thank the College of Life Sciences at Shaanxi Normal University for the sharing platform of laboratory apparatus. This work was funded by the National Natural Science Foundation of China (81972417), The “1000 Young Scholars” Program of Shaanxi Province, Natural Science Foundation of Shaanxi Province (2020JM-292, 2020JQ-430), Fundamental Research Funds for the Central Universities (GK201902002, GK201903061) and College Students’ Innovative Entrepreneurial Training Plan Program (S202010718091).

Author contributions

P.G., and X.M.D. supervised the project, designed the studies, and wrote the manuscript. P.G., J.L.H., Q.W.X., G.Q.H., B.B.X., H.H., and N.E.S performed the experiments.

Competing financial interests

The authors declare no competing financial interests.

References

1. Song B, Park S-H, Zhao JC, Fong K, Li S, Lee Y, et al. Targeting FOXA1-mediated repression of TGF-β signaling suppresses castration-resistant prostate cancer progression. Journal of Clinical Investigation. 2018;129:569–82.
2. van der Toom EE, Axelrod HD, de la Rosette JJ, de Reijke TM, Pienta KJ, Valkenburg KC. Prostate-specific markers to identify rare prostate cancer cells in liquid biopsies. Nat Rev Urol. 2019;16:7–22.
3. Liu XS, Song B, Elzey BD, Ratliff TL, Konieczny SF, Cheng L, et al. Polo-like Kinase 1 Facilitates Loss of Pten Tumor Suppressor-induced Prostate Cancer Formation. Journal of Biological Chemistry. 2011;286:35795–800.
4. Zhang Z, Hou X, Shao C, Li J, Cheng J-X, Kuang S, et al. Plk1 Inhibition Enhances the Efficacy of Androgen Signaling Blockade in Castration-Resistant Prostate Cancer. Cancer Res. 2014;74:6635–47.
5. Weichert W, Schmidt M, Gekeler V, Denkert C, Stephan C, Jung K, et al. Polo-like kinase 1 is overexpressed in prostate cancer and linked to higher tumor grades. Prostate. 2004;60:240–5.
6. Strebhardt K, Ullrich A. Targeting polo-like kinase 1 for cancer therapy. Nat Rev Cancer. 2006;6:321–30.
7. García IA, Garro C, Fernandez E, Soria G. Therapeutic opportunities for PLK1 inhibitors: Spotlight on BRCA1-deficiency and triple negative breast cancers. Mutation Research/Fundamental and Molecular Mechanisms of Mutagenesis. 2020;821:111693.
8. Ding Z, Wu C-J, Chu GC, Xiao Y. SMAD4-dependent barrier constrains prostate cancer growth and metastatic progression. Nature. 2011;470:269–73.
9. Tan J, Li Z, Lee PL, Guan P, Aau MY, Lee ST, et al. PDK1 Signaling Toward PLK1–MYC Activation Confers Oncogenic Transformation, Tumor-Initiating Cell Activation, and Resistance to mTOR-Targeted Therapy. Cancer Discovery. 2013;3:1156–71.
10. Shi C, Yang EJ, Liu Y, Mou PK, Ren G, Shim JS. Bromodomain and extra-terminal motif (BET) inhibition is synthetic lethal with loss of SMAD4 in colorectal cancer cells via restoring the loss of MYC repression. Oncogene. 2021;40:937–50.
11. Adham IM, Sallam MA, Steding G, Korabiowska M, Brinck U, Hoyer-Fender S, et al. Disruption of the *Pelota* Gene Causes Early Embryonic Lethality and Defects in Cell Cycle Progression. Mol Cell Biol. 2003;23:1470–6.
12. Davis L, Engebrecht J. Yeast dom34 Mutants Are Defective in Multiple Developmental Pathways and Exhibit Decreased Levels of Polyribosomes. Genetics. 1998;149:45–56.
13. Pedersen K, Canals F, Prat A, Tabernero J, Arribas J. PELO negatively regulates HER receptor signalling and metastasis. Oncogene. 2014;33:1190–7.
14. Chen S, Bartkovitz D, Cai J, Chen Y, Chen Z, Chu XJ, et al. Identification of novel, potent and selective inhibitors of Polo-like kinase 1. Bioorg Med Chem Lett. 2012;22(2):1247-1250.
15. Gheghiani L, Wang L, Zhang Y, Moore XTR, Zhang J, Smith SC, et al. PLK1 Induces Chromosomal Instability and Overrides Cell-Cycle Checkpoints to Drive Tumorigenesis. Cancer Res. 2021;81(5):1293-1307.

16. Kamisawa T, Wood LD, Itoi T, Takaori K. Pancreatic cancer. Lancet. 2016;388(10039):73-85.
17. Ogawa R, Yamamoto T, Hirai H, Hanada K, Kiyasu Y, Nishikawa G, et al. Loss of SMAD4 Promotes Colorectal Cancer Progression by Recruiting Tumor-Associated Neutrophils via the CXCL1/8-CXCR2 Axis. Clin Cancer Res. 2019;25(9):2887-2899.
18. Yao Y, Zhang Z, Kong F, Mao Z, Niu Z, Li C, et al. Smad4 induces cell death in HO-8910 and SKOV3 ovarian carcinoma cell lines via PI3K-mTOR involvement. Exp Biol Med (Maywood). 2020;245:777–84.
19. Zhang M, Singh R, Peng S, Mazumdar T, Sambandam V, Shen L, et al. Mutations of the LIM protein AJUBA mediate sensitivity of head and neck squamous cell carcinoma to treatment with cell-cycle inhibitors. Cancer Letters. 2017;392:71–82.
20. Liakath-Ali K, Mills EW, Sequeira I, Lichtenberger BM, Pisco AO, Sipilä KH, et al. An evolutionarily conserved ribosome-rescue pathway maintains epidermal homeostasis. Nature. 2018;556:376–80.
21. Whittaker SR, Mallinger A, Workman P, Clarke PA. Inhibitors of cyclin-dependent kinases as cancer therapeutics. Pharmacol Ther. 2017;173:83-105.
22. Drucker DJ. Advances in oral peptide therapeutics. Nat Rev Drug Discov. 2020;19(4):277-289.
23. Fosgerau K, Hoffmann T. Peptide therapeutics: current status and future directions. Drug Discovery Today. 2015;20:122–8.
24. Olmos D, Barker D, Sharma R, Brunetto AT, Yap TA, Taegtmeyer AB, et al. Phase I study of GSK461364, a specific and competitive Polo-like kinase 1 inhibitor, in patients with advanced solid malignancies. Clin Cancer Res. 2011;17(10):3420-30.
25. García IA, Garro C, Fernandez E, Soria G. Therapeutic opportunities for PLK1 inhibitors: Spotlight on BRCA1-deficiency and triple negative breast cancers. Mutat Res. 2020;821:111693.
26. Kumar S, Kim J. PLK-1 Targeted Inhibitors and Their Potential against Tumorigenesis. Biomed Res Int. 2015;705745.
27. Goroshchuk O, Kolosenko I, Vidarsdottir L, Azimi A, Palm-Apergi C. Polo-like kinases and acute leukemia. Oncogene. 2019;38(1):1-16.
28. Dong X, Zhao K, Zheng W, Xu C, Zhang M, Yin R, et al. EDAG mediates Hsp70 nuclear localization in erythroblasts and rescues dyserythropoiesis in myelodysplastic syndrome. FASEB j. 2020;34:8416–27.
29. Gao P, Xia J-H, Sipeky C, Dong X-M, Zhang Q, Yang Y, et al. Biology and Clinical Implications of the 19q13 Aggressive Prostate Cancer Susceptibility Locus. Cell. 2018;174:576-589.e18.
30. Cerami E, Gao J, Dogrusoz U, Gross BE, Sumer SO, Aksoy BA, et al. The cBio Cancer Genomics Portal: An Open Platform for Exploring Multidimensional Cancer Genomics Data: Figure 1. Cancer Discovery. 2012;2:401–4.
31. Gao J, Aksoy BA, Dogrusoz U, Dresdner G, Gross B, Sumer SO, et al. Integrative Analysis of Complex Cancer Genomics and Clinical Profiles Using the cBioPortal. Science Signaling. 2013;6:pl1–pl1.

32. Barrett T, Wilhite SE, Ledoux P, Evangelista C, Kim IF, Tomashevsky M, et al. NCBI GEO: archive for functional genomics data sets—update. Nucleic Acids Research. 2012;41:D991–5.

33. Edgar R. Gene Expression Omnibus: NCBI gene expression and hybridization array data repository. Nucleic Acids Research. 2002;30:207–10.

Figures

Figure. 1

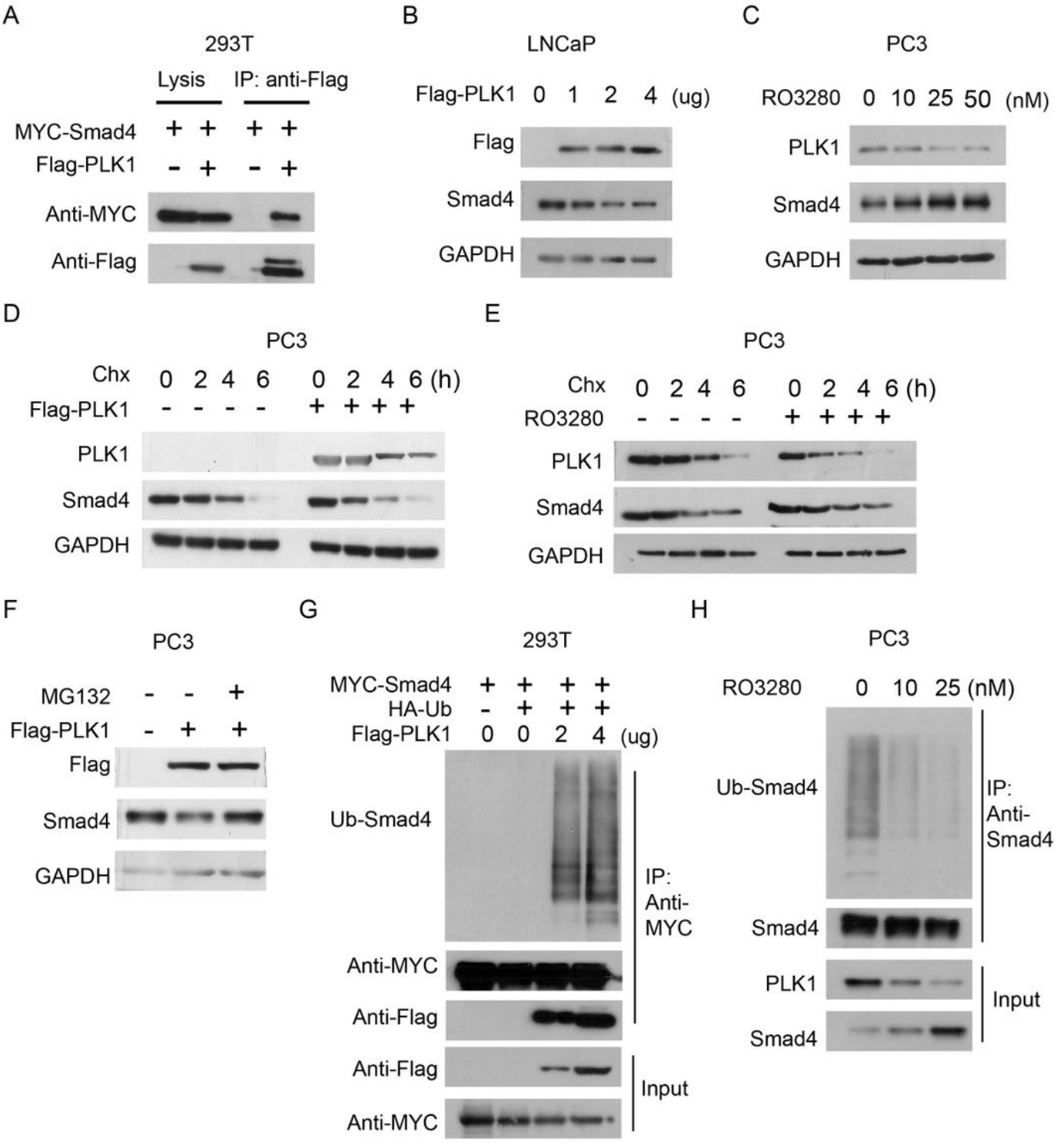

Figure 1

PLK1 promoted the ubiquitination and degradation of Smad4 in prostate cancer A, HEK293T cells were transfected with Myc-tagged Smad4 and Flag-tagged PLK1 expression plasmids as indicated, whole cell lysates were extracted and immunoprecipitated with anti-Flag antibodies. B, LNCaP cells were transfected with increasing amounts of Flag-PLK1 expression plasmids as indicated. The Smad4 protein level was assessed by immunoblotting. GAPDH was used as a loading control. C, PC3 cells were treated with increasing amounts of RO3280 as indicated. The protein levels of PLK1 and Smad4 were analyzed by immunoblotting. D, PC3 cells transfected with Flag-PLK1 or control vector were treated with 50 μg/mL cycloheximide (CHX) for the indicated times and then analyzed by western blot. E, PC3 cells were treated with RO3280 for 12 h, followed by treatment with 50 μg/mL CHX for the indicated times. The protein levels of PLK1 and Smad4 were assessed by western blot. F, PC3 cells transfected with Flag-PLK1 or control vector were treated with or without MG132 (20 μM) for 8 hours. Cell lysates were subjected to immunoblot with Flag or Smad4 antibody. G, HEK293T cells were transfected with increasing amounts of Flag-PLK1 together with HA-Ub and Myc-Smad4. Immunoprecipitation was performed with anti-Myc antibody, and subjected to western blot with anti-HA, Myc or Flag antibody. H, HEK293T cells were treated with various amounts of RO3280 for 12 h. Then cells were harvested for immunoprecipitation and immunoblot analysis using the indicated antibodies. Ubiquitin antibody was used to detect endogenous ubiquitinated Smad4.

Figure. 2

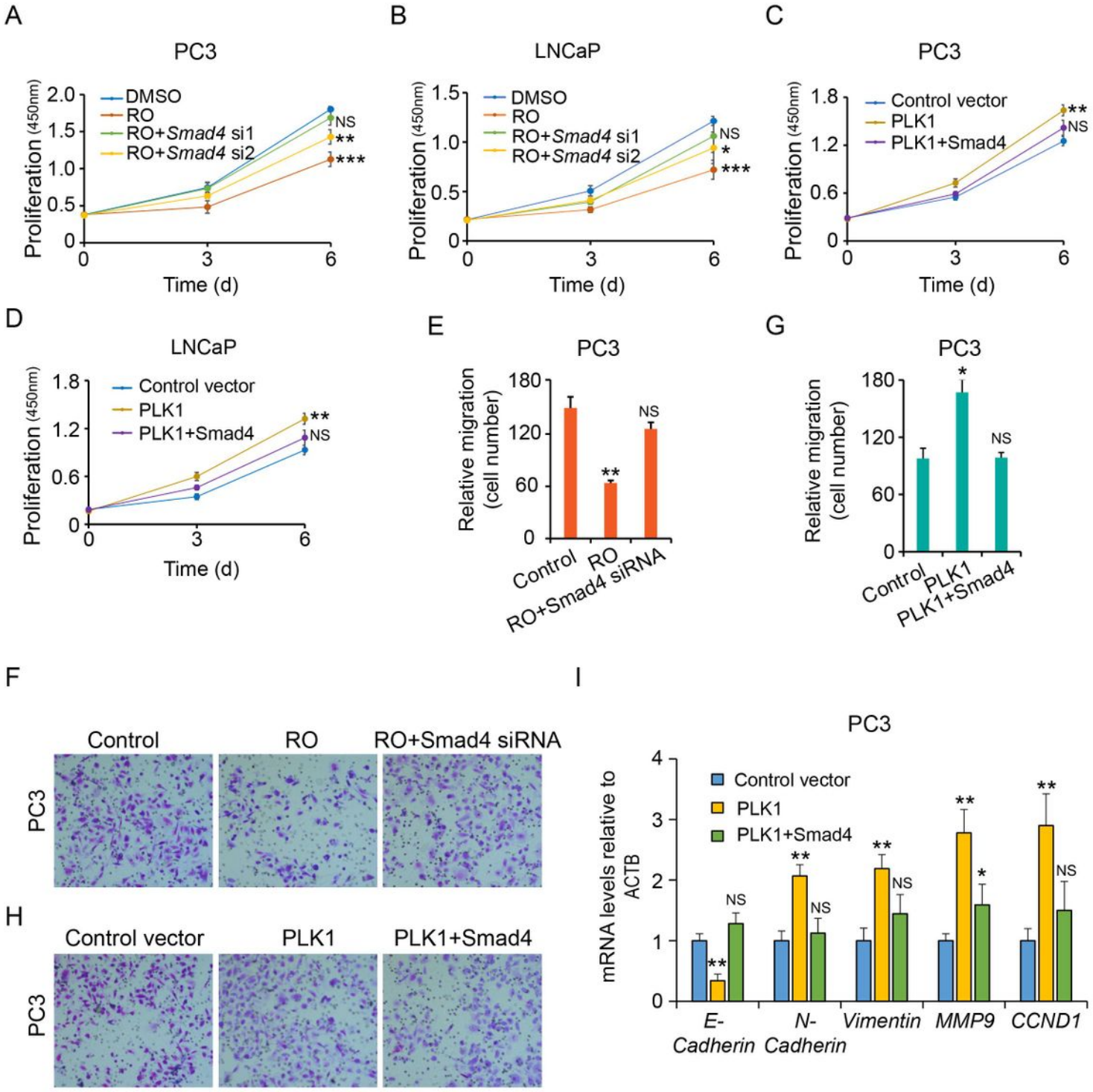

Figure 2

Smad4 reversed the biological function of PLK1 in prostate cancer A-B, PC3 (A) or LNCaP cells (B) were treated with RO3280 for 12 h, followed by transfection with Smad4 siRNA. Then cell proliferation was measured by XTT colorimetric assays (mean ± SD of triplicate experiments). C-D, PC3 cells (C) or LNCaP cells (D) stably expressing control or PLK1 plasmid were transiently transfected with Smad4 plasmid. Then cell proliferation was measured by XTT colorimetric assays (mean ± SD of triplicate experiments).

E-F, Quantification analysis of migration assays (E) and representative Trans-well data of migration assays (F) in PC3 cells treated with RO3280 for 12 h, followed by transfected with Smad4 siRNA. G-H, Quantification analysis of migration assays (G) and representative Trans-well data of migration assays (H) in PC3 cells stably expressing control or PLK1 plasmid, followed by transfected with Smad4 plasmid. I, Real-time RT-PCR analysis of mRNA level of different EMT markers and CCND1 in the indicated cells. Data are represented as means ± S.D. *p < 0.05; **p < 0.01; ***p < 0.001.

Figure. 3

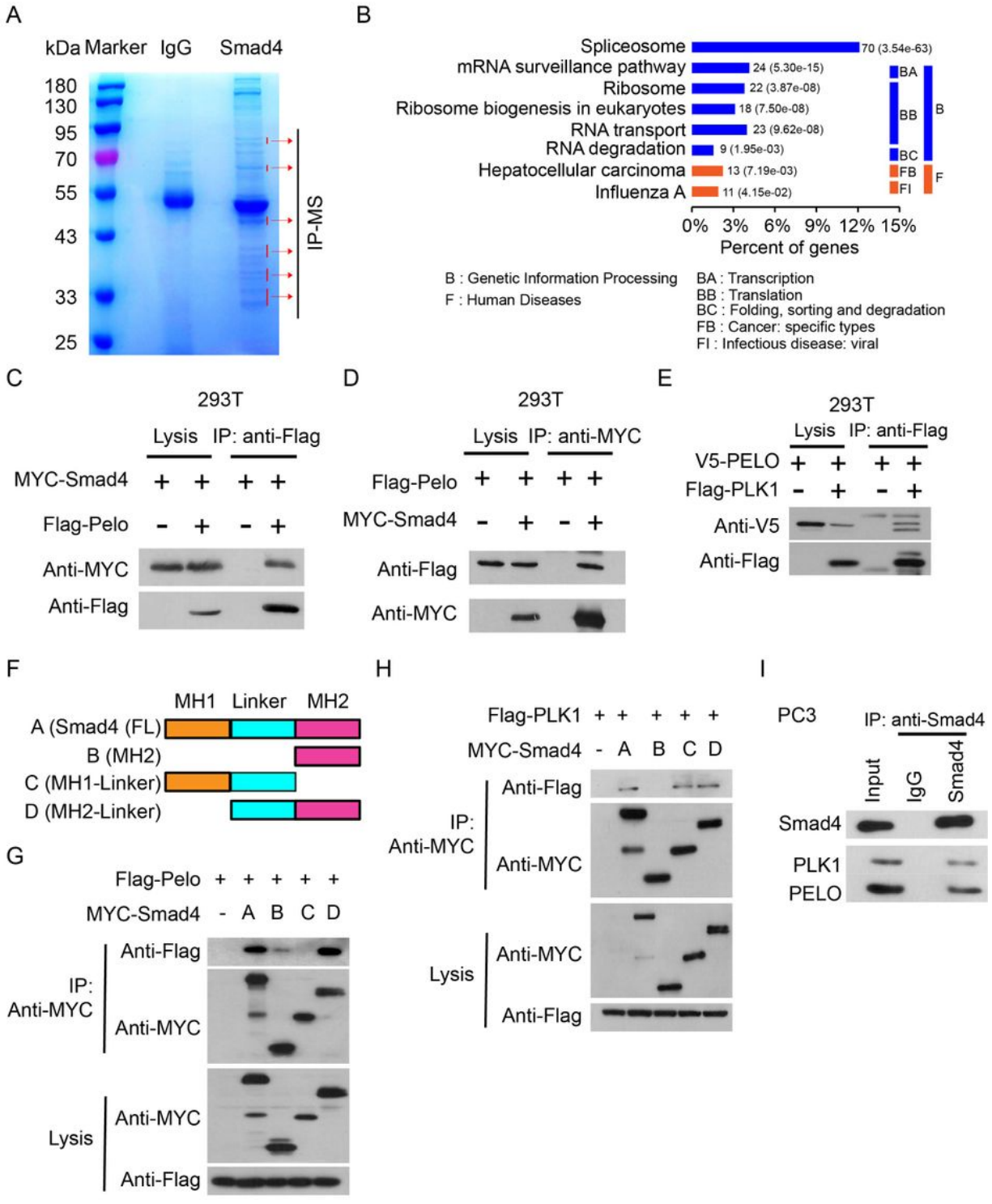

Figure 3

PLK1 formed a protein complex with Smad4 and PELO in PCa A, Coomassie blue staining of coimmunoprecipitated mixtures separated by SDS-PAGE; bands were cut from the gel as indicated, digested with trypsin, and subjected to LC/MS. B, Molecular function categories for potential Smad4 interacting proteins. C-D, 293T cells were transfected with Myc-tagged Smad4 and Flag-tagged PELO expression plasmids as indicated, whole cell lysates were extracted and immunoprecipitated with anti-Flag antibodies (C) or anti-Myc antibodies (D). E, 293T cells were transfected with V5-PELO and Flag-PLK1 expression plasmids as indicated, and whole cell lysates were extracted and immunoprecipitated with anti-Flag antibodies. F, The schematic illustration of Smad4 and its truncated fragments were shown. G-H, Mapping the binding domain of Smad4 with PELO (G) or PLK1 (H). HEK293T cells were transiently co-transfected with the expression vectors as indicated. After 24 h, cell lysates were prepared and immunoprecipitations were performed with anti-Myc antibody. Immunoprecipitants were analyzed with anti-Flag antibody and anti-Myc antibody. I, PC3 cells extracts were immunoprecipitated with Smad4 antibody, and the immunoprecipitated proteins were analyzed by Western blotting.

Figure. 4

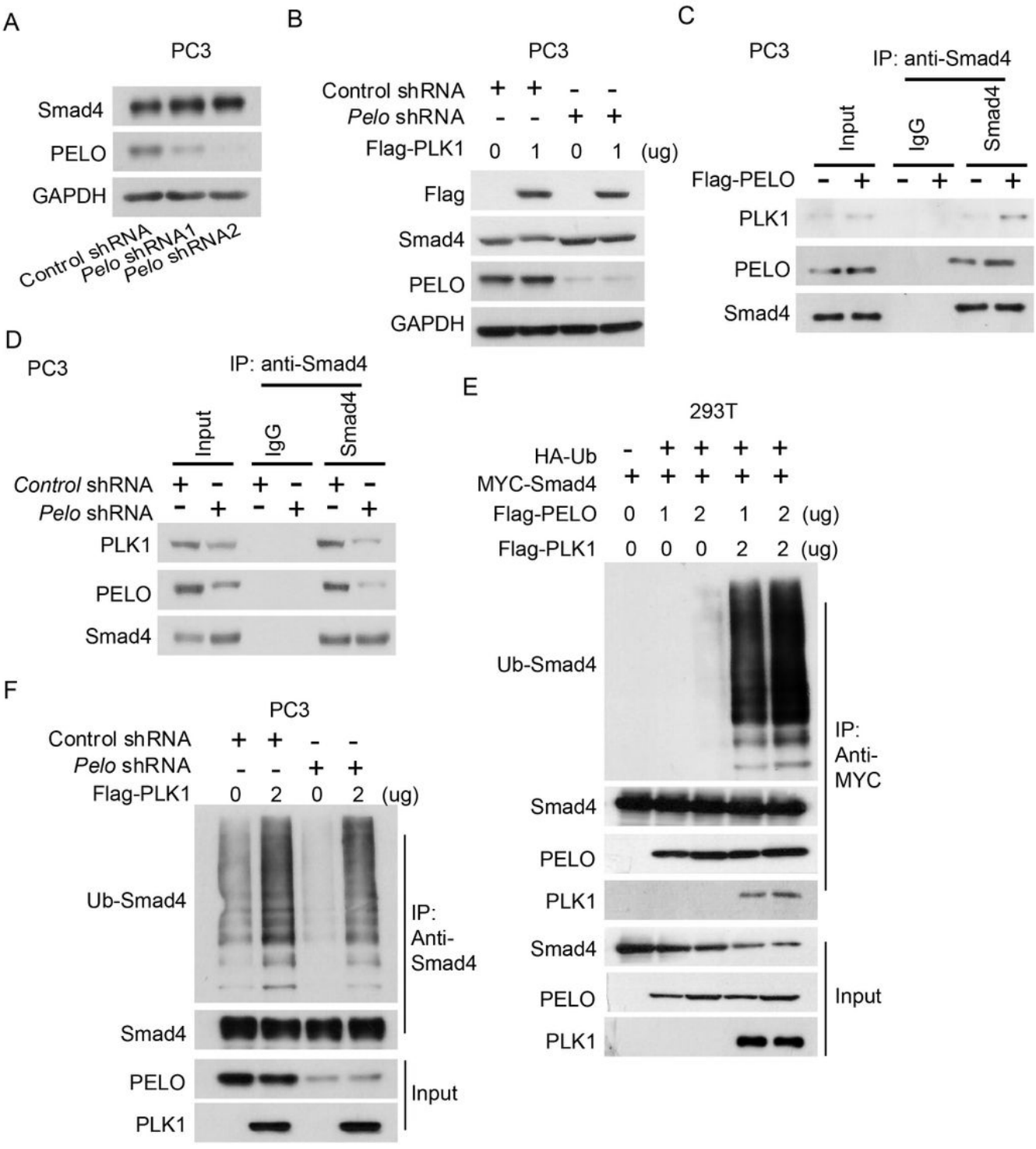

Figure 4

PELO facilitated PLK1-induced the ubiquitination and degradation of Smad4 A, Western blotting analysis of Smad4 and PELO expression in PELO depleted PC3 cells. GAPDH was used as a loading control. B, Control or PELO depleted PC3 cells were transfected with PLK1 plasmid. Cell lysates were subjected to immunoblot with Flag, Smad4 and PELO antibody. C-D, The whole cell lysates were prepared from PC3 cells transfected with PELO overexpression lentivirus (C) or PELO shRNA lentivirus (D), and

immunoprecipitations were performed with indicated antibodies. E, HEK293T cells were transfected with the indicated plasmids, including HA-Ub, Myc-Smad4, Flag-PELO and Flag-PLK1. Immunoprecipitation and immunoblot analysis were performed with the indicated antibodies. F, Control or PELO depleted PC3 cells were transfected with PLK1 plasmid. The ubiquitination of Smad4 was analyzed by immunoprecipitation and Western blot with indicated antibodies.

Figure. 5

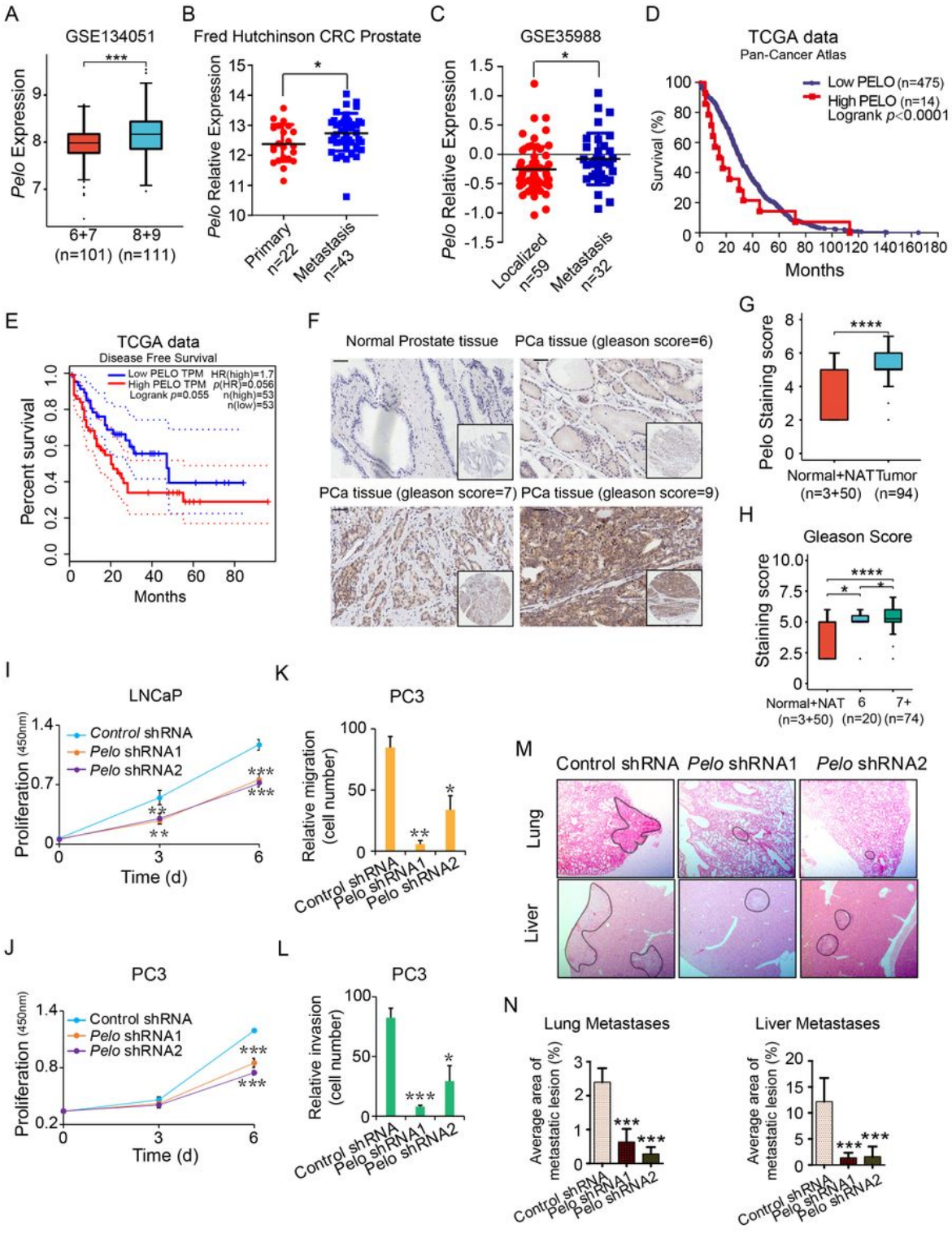

Figure 5

Increased expression of PELO positively associated with high risk of PCa A, PELO mRNA expression in prostate cancer tissues with different Gleason score from GEO (GSE134051) database. B, PELO mRNA expression in localized and metastatic tissues of prostate cancer from Fred Hutchinson CRC prostate. C, PELO mRNA expression in localized and metastatic tissues of prostate cancer from GEO databases GSE35988. D, Association between overall survival of prostate cancer patients and PELO mRNA expression from the TCGA database. E, Association between disease-free survival of prostate cancer patients and PELO mRNA expression from the TCGA database. F, Representative pictures of PELO protein expression in prostate cancer tissue chip detected by IHC. G-H, Quantification of PELO protein in prostate cancer. Scale bar =100 μm. I-J, Knockdown of PELO reduces PCa cell proliferation measured by XTT colorimetric assays (mean ± SD of triplicate experiments) in LNCaP cells (I) and PC3 cells (J). K-L, Quantification analysis of migration (K) and invasion (L) assays in PC3 cells transfected with PELO shRNA (PELO shRNA1, PELO shRNA2) or control shRNA. M, Representative H&E images of lung and liver metastases in all five groups of mice at 5× magnification, respectively. Dotted circles represent metastatic lesions. Scale bars, 500 μm. N, Bar graph represents an average area in percentage of metastatic lesions within the lung and liver in the aforementioned groups, n = 5. *p < 0.05; **p < 0.01; ***p < 0.001.

Figure. 6

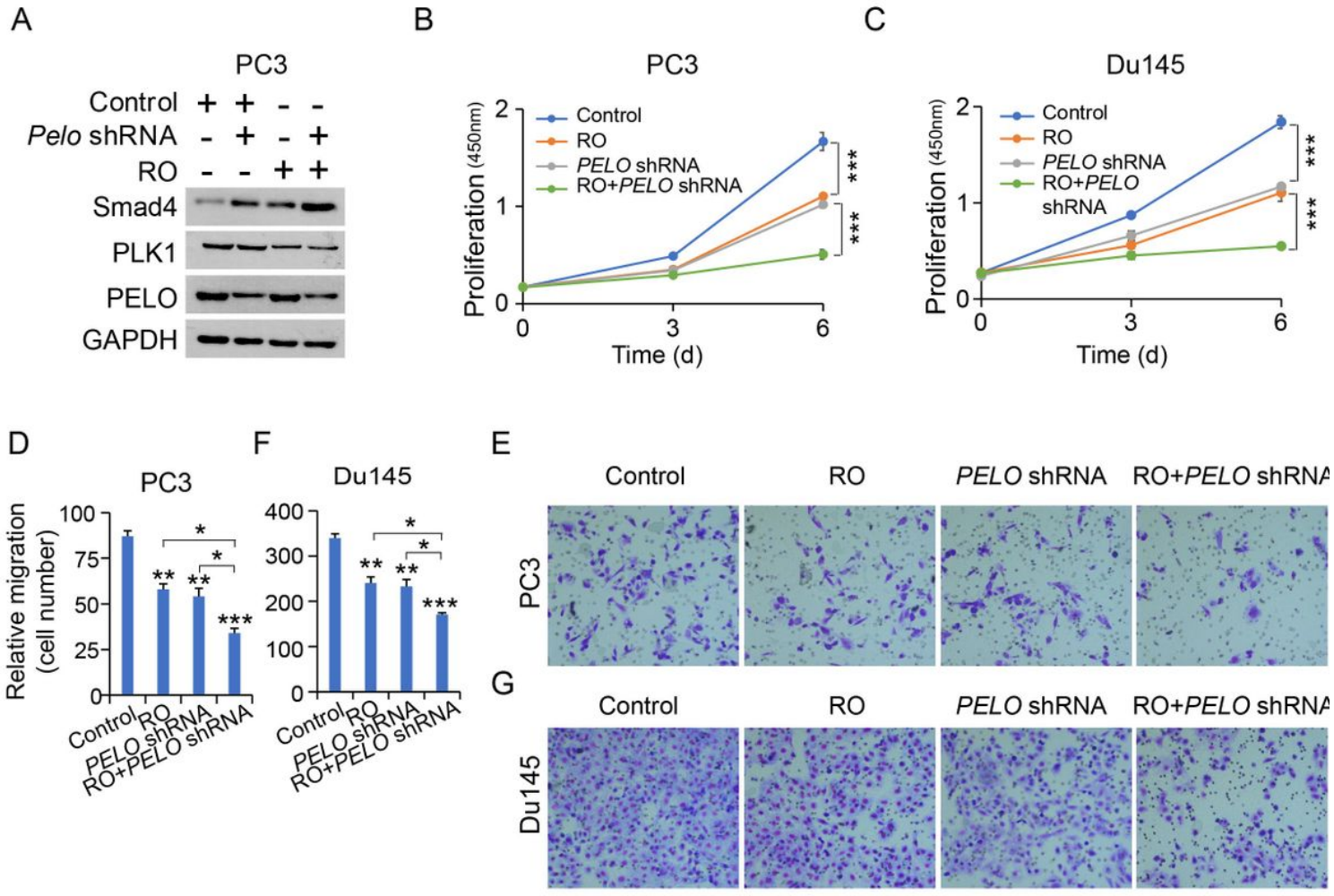

Figure 6

Knockdown of PELO enhanced the tumor suppressive function of PLK1 inhibitor RO A, PC3 cells were transfected with PELO shRNA lentivirus or control lentivirus, followed by treatment with RO3280 and then analyzed by western blot. GAPDH was used as a loading control. B, Cell proliferation assays in PC3 cells treated with RO3280 or stably transfected with PELO shRNA lentivirus as in (B). C, Cell proliferation assays in Du145 cells treated with RO3280 or stably transfected with PELO shRNA lentivirus as in (C). D-E, Quantification analysis (D) and representative pictures (E) of migration assays in PC3 cells treated with RO3280 or stably transfected with PELO shRNA lentivirus as in (D, E). F-G, Quantification analysis (F) and representative pictures (G) of migration assays in Du145 cells treated with RO3280 or stably transfected with PELO shRNA lentivirus as in (E, F). *$p < 0.05$; **$p < 0.01$; ***$p < 0.001$.

Figure. 7

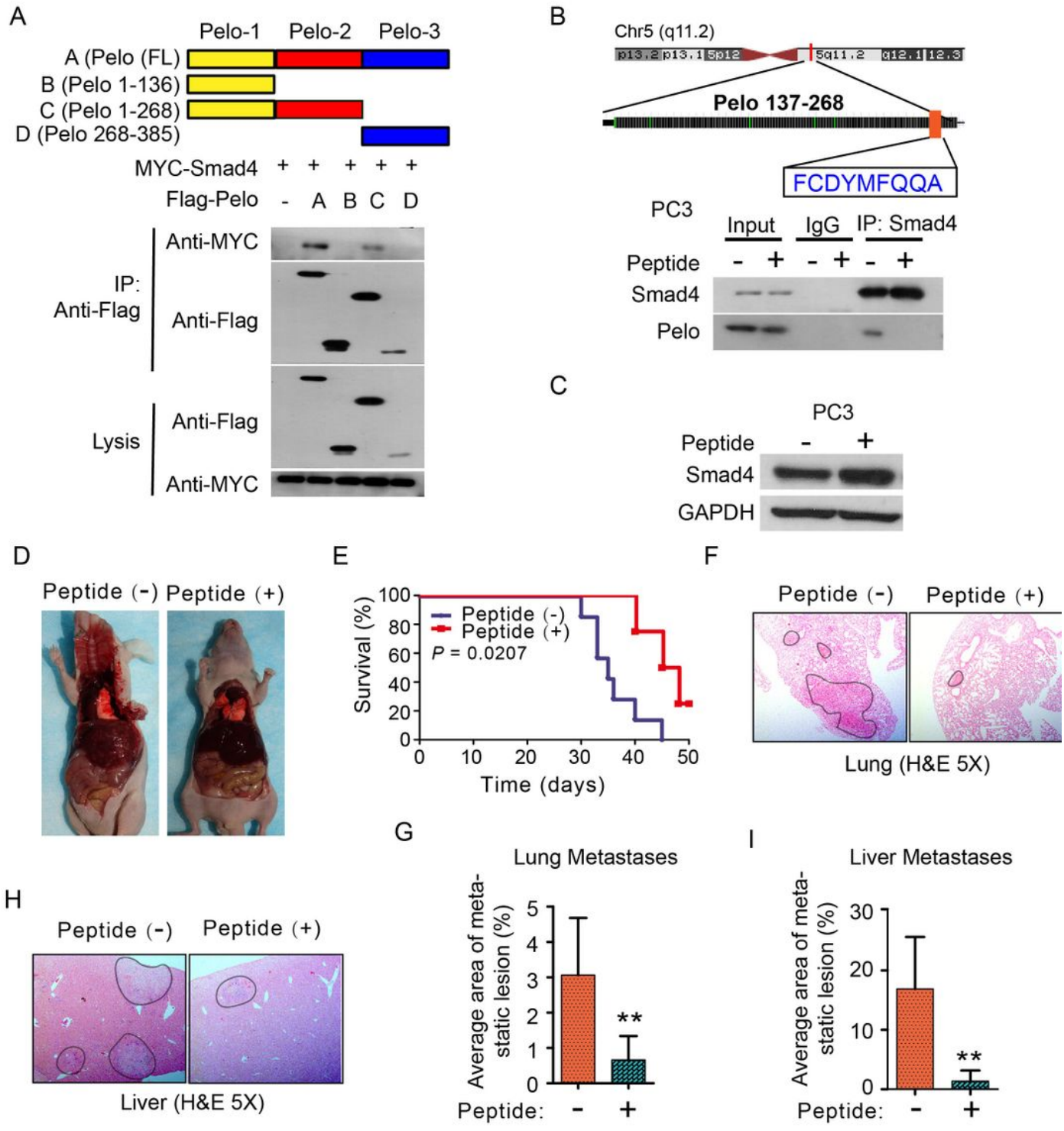

Figure 7

Blocking interaction between PELO and Smad4 by specific peptide markedly inhibited PCa cell metastasis A, HEK293T cells were co-transfected with Smad4 and the deletion mutants of PELO with Flag tag. After 24 h of transfection, cell lysates were prepared, and immunoprecipitations were performed with anti-Flag antibody. Immunoprecipitants were analyzed with anti-Flag antibody and anti-Myc antibody. The schematic illustration of PELO and its truncated fragments were shown in the right upper

panel. B, Peptide localized at PELO-2 domain can block the interaction between Smad4 and PELO in PC3 cells. C, PC3 cells were treated with Peptide and the protein level of Smad4 was analyzed by western blot. D, Mice (n = 8) that injected with peptide via tail vein at a dose of 10 mg/kg significantly suppressed lung and liver metastases compared with mice injected with PBS (n = 7). E, Mice (n = 8) that injected with peptide via tail vein at a dose of 10 mg/kg remarkably reduced survival rate compared with mice injected with PBS (n = 7). Survival Differences were evaluated with the log-rank test. F, Representative H&E images of lung metastases in two groups of mice at 5× magnification. Dotted circles represent metastatic lesions. Scale bars, 500 μm. G, Bar graph represents an average area in percentage of metastatic lesions within the lung in the aforementioned groups, peptide (-) group: n = 7; peptide (+) group: n = 8. H, Representative H&E images of liver metastases in two groups of mice at 5× magnification. Dotted circles represent metastatic lesions. Scale bars, 500 μm. I, Bar graph represents an average area in percentage of metastatic lesions in liver in the aforementioned groups, peptide (-) group: n = 7; peptide (+) group: n = 8. **p < 0.01.

Supplementary Files

This is a list of supplementary files associated with this preprint. Click to download.

- supplFigurelegend.docx